Computational study of transition dynamics in 55-atom clusters

Frank H. Stillinger and Dorothea K. Stillinger
AT&T Bell Laboratories, Murray Hill, New Jersey 07974

(Received 17 May 1990; accepted 16 July 1990)

Molecular dynamics computer simulation has ben employed to study structure and isomerization dynamics of intact 55-atom clusters. The interactions used were selected to represent the heavier noble gases Ar, Kr, and Xe. As an aid for interpretation of results, the molecular dynamics computation was coupled to steepest-descent mapping to locate relevant cluster inherent structures (potential energy minima). A relatively sharp melting transition has been reproducibly observed. In its low-temperature "solid state" the cluster predominately inhabits the basins for the Mackay icosahedral inherent structure, with occasional excursions into and out of particle–hole states (an atom promoted from filled second to empty third icosahedral shell). Most inherent structures for the liquid droplet state are amorphous, are higher in energy than those for the solid, have no obvious icosahedral ancestry, and display surface capillary excitations. Freezing can produce defective solid structures which then can be annealed to the ground-state icosahedral structure. Root-mean-square distances under mapping to minima have been evaluated vs temperature; they show behavior qualitatively similar to, but quantitatively shifted from, the bulk-phase behavior prescribed by the Lindemann melting criterion and its conjugate freezing criterion.

I. INTRODUCTION

Understanding the properties of small gas-phase clusters offers several significant benefits. First, these clusters provide a bridge between the regimes of single atoms, ions, or molecules on the one hand, to macroscopic condensed phases on the other hand.[1,2] Second, they offer natural examples of dynamical systems with relatively few degrees of freedom within which various energy transfer processes can be examined.[3,4] Third, they play a fundamental role in nucleation phenomena.[5,6] Fourth, they can serve as catalytic media for chemical reactions.[7]

The structural chemistry of small atomic clusters has proven to be surprisingly complex. For example, the recent *ab initio* calculations by Raghavachari and Rohlfing for neutral silicon clusters Si_n, $n \leqslant 11$, fail to exhibit bonding geometry of the type present in the cubic macroscopic crystal of that substance.[8,9] Similar discrepancies obtain for other elements as well.[10,11]

Under these circumstances it seems prudent for the moment to keep details of structural chemistry separated from the statistical mechanical phenomena associated with thermally activated processes, in particular cluster melting and freezing kinetics. To concentrate on the latter, then, it is advisable to restrict attention to relatively simple Hamiltonian models. That is the course selected for the present work. Eventually it should become possible to reattach structural and statistical advances to achieve a more comprehensive understanding of gas phase clusters.

This paper reports results from a classical molecular dynamics study of a model whose interparticle interactions are appropriate for the heavier noble gases (Ar, Kr, Xe). The model is specified in Secs. II and III, and has previously been used to examine bulk-phase properties of the noble gases.[12–15]

Our calculations have been largely confined to clusters containing 55 particles. For noble gas interactions this integer is one of the icosahedral magic numbers of the form

$$N(n) = \tfrac{1}{3}(2n+1)(5n^2+5n+3); \qquad (1.1)$$

the ground-state structures of clusters comprising these integer numbers of atoms are the so-called Mackay polyhedra.[16] Here n indexes the number of closed icosahedral shells outside of the single central particle.

The molecular dynamics protocol employed is described below in Sec. II. We have found it extremely useful in the present context to invoke a configurational mapping procedure that was originally devised to probe phenomena in extended condensed phases.[17–19] This involves connecting any instantaneous dynamical configuration of the particles to a local potential energy minimum, the "inherent structure." Details of the mapping technique also appear in Sec. II. The first application of this mapping to minima for clusters apparently occurred in study of ice crystallites and their melting.[20] More recently several research groups[21–24] have begun to utilize the same tool to describe some aspects of noble gas clusters of various sizes, though not in the same detail as examined below.

Just as previous simulations have shown,[23] our 55-particle cluster exhibits a relatively sharp and distinctive melting transition. This is revealed by the existence of two principal branches to the thermal (caloric) equation of state, discussed in Sec. IV. Both branches manifest substantial vibrational anharmonicity, but the mapping to minima reveals a fundamental difference in the inherent structures represented by the "solid" and "liquid" branches.

Details involved in kinetics of the cluster "phase transition" appear in Sec. V. The mapping to minima helps to clarify the structural basis for hysteresis observed in successive melting and freezing cycles. Furthermore, it aids in the interpretation of the transition entropy.

It has been pointed out before that the concept of inherent structures for condensed phases provides a novel inter-

 0021-9606/90/206013-12$03.00

pretation of the Lindemann melting criterion for solids, and leads immediately and naturally to a complementary freezing criterion for liquids.[25] Section VI shows how this notion can be adapted to clusters, and reinforces the view of the $N=55$ cluster transition as a small-system version of the first-order liquid-crystal phase change.

Our final section, Sec. VII, offers a few general observations and concluding remarks.

II. DYNAMICAL MODEL

We study the classical dynamics of N ($=55$) point particles that interact through a potential energy function:

$$\Phi(\mathbf{r}_1\cdots\mathbf{r}_N)=\sum_{i<j} v_5(r_{ij}). \tag{2.1}$$

The pair potential v_5 has derivatives of all orders for $r>0$, but vanishes identically beyond a cutoff distance a:

$$\begin{aligned} v_5(r) &= A(r^{-12}-r^{-5})\exp[(r-a)^{-1}] \quad (0<r<a), \\ &= 0 \quad (a\leqslant r); \end{aligned} \tag{2.2}$$

$$A=6.767\,441, \quad a=2.464\,918\,32.$$

The numerical values shown for A and a were selected so that v_5 would display some of the same properties as the Lennard-Jones potential

$$v_{\mathrm{LJ}}(r)=4(r^{-12}-r^{-6}). \tag{2.3}$$

Specifically both v_5 and v_{LJ} vanish at $r=1$, and both have minima of depth -1 at

$$r_e=2^{1/6}=1.122\,462\,048\ \ldots. \tag{2.4}$$

As regards the successful representation of real noble gas behavior, v_5 offers a significant advantage of v_{LJ}: only the former produces the observed face-centered-cubic (fcc) structure as the stable crystal form at low temperature, while the latter erroneously predicts that the hexagonal close-packed (hcp) structure would appear.[25,26]

For comparison with the equilibrium dimer distance in Eq. (2.4) it might be noted in passing that the nearest-neighbor spacing in the zero-temperature, zero-pressure fcc crystal with v_5 interactions is

$$r_{\mathrm{cr}}=1.098\,709\ \ldots. \tag{2.5}$$

The corresponding cohesive energy per atom in this structure is

$$\Phi(\mathrm{fcc})/N=-7.162\,077\ \ldots. \tag{2.6}$$

The classical Newton equations of motion for our cluster system have been numerically integrated using the standard Gear algorithm in fifth order.[27,28] For technical reasons we have elected to use periodic boundary conditions with a large cubical unit cell ($L=20.0$). The cluster configurations encountered during the simulation are all sufficiently compact that the cluster cannot interact with its periodic images in neighboring cells. The cluster center of mass has been constrained to a fixed position near the cell center, so that cluster temperature during any simulation run was inferred from the mean value of the kinetic energy (KE) for that run as follows:

$$k_B T=2\langle \mathrm{KE}\rangle/3(N-1), \tag{2.7}$$

where k_B is Boltzmann's constant. Angular momentum was not constrained. Total energy (and thus the temperature) was adjusted between runs by the standard velocity scaling method; during any given run total energy would typically be conserved to at least seven significant figures.

At various regular and frequent intervals during some of the simulation runs the instantaneous configuration was mapped onto the relative Φ minimum within whose "basin of attraction" the dynamical system happened to find itself. This configurational quenching operation in principle requires finding the $u\rightarrow+\infty$ solution to the simultaneous relaxation equations:

$$d\mathbf{r}_i/du=-\nabla_i\Phi(\mathbf{r}_1\cdots\mathbf{r}_N), \tag{2.8}$$

where the Newtonian configuration supplies the initial($u=0$) condition. This mapping procedure in no way disturbs the Newtonian cluster dynamics, but is treated as a parallel numerical operation. Solutions to Eq. (2.8) have been obtained using the MINOP procedure.[29]

The entire numerical program is carried out in dimensionless form, using the reduced pair potential (2.2) and unit mass for all atoms. In order to interpret results properly in terms of specific noble gases, it is necessary to redimension the quantities calculated. Table I lists the appropriate length (σ), energy (ϵ), and mass (m) to use for redimensioning in the cases of Ar, Kr, and Xe, respectively. It also presents the corresponding time units that can be constructed from these parameters:

$$\tau=\sigma(m/\epsilon)^{1/2}. \tag{2.9}$$

It might be noted that the period of harmonic vibration for a dimer with interaction v_5 is 0.82749τ.

A sufficiently short time increment Δt must be chosen to guarantee that the numerical integration of the Newton equations conserves energy accurately. We have found that $\Delta t=0.005\tau$ suffices for clusters at low temperature, but that Δt must be reduced to 0.00125τ for the high temperature regime above the cluster melting point.

III. INHERENT CLUSTER STRUCTURES

A preliminary discussion of stable isomeric forms (inherent structures) for the 55-atom cluster is warranted before examining molecular dynamics results. The number of distinct structures is unknown, but it seems reasonable to suppose that it rises with N in an approximately exponential manner for any given interaction potential. Hoare[30] has enumerated inherent structures for v_{LJ} with $N\leqslant 13$; his results for the larger N values conform roughly to the expression

$$2.4444\times10^{-3}\ \exp[0.993\,05N]. \tag{3.1}$$

TABLE I. Scale parameters for noble gases.

	Ar	Kr	Xe
σ (Å)	3.40	3.60	4.10
ϵ (K)	120.	171	221
m (10^{-23} g)	6.6336	13.916	21.803
τ (ps)	2.152	2.764	3.466

Formal extension of this function to $N = 55$ yields the estimate 1.283×10^{21}. Since v_{LJ} and v_5 are qualitatively similar, this number can be taken as a crude estimate of the number of distinct inherent structures for the $N = 55$, v_5 clusters.

Figure 1 displays the icosahedral ground state for our 55-atom cluster with v_5 pair interactions. The view shown clearly illustrates the fivefold rotational symmetry that exists at each of the 12 vertex particles in the outer shell. This outer shell, containing 42 particles in all, rests on an inner icosahedral shell of 12 particles that are hidden from view in Fig. 1. A single particle lies buried at the center.

The potential energy of this icosahedral ground state is

$$\Phi_{55}(\text{icos}) = -256.362\,271\ \ldots . \tag{3.2}$$

The corresponding value for v_{LJ} is $-279.248\ \ldots$.

Each of the icosahedral Mackay polyhedra can be rearranged into a cuboctahedral fragment of the face-centered-cubic crystal that supplies the global Φ minimum in the large-N limit.[16] At least for v_{LJ} it has been established that the icosahedra remain lowest in energy for all magic numbers $N(n)$, $n < 14$, but that for larger n the cuboctahedral form prevails.[31] When $n = 1$, the 13-particle cuboctahedral form is not even a local minimum, but a saddle point on the multidimensional Φ hypersurface. Adding the next shell however confers local stability. Figure 2 illustrates the resulting cuboctahedral inherent structure, for which

$$\Phi_{55}(\text{cubo}) = -246.248\,674\ \ldots . \tag{3.3}$$

Locating with confidence the highest-lying relative minimum for Φ, the least stable inherent structure for the cluster, seems to be a difficult task. Nevertheless an estimate of where this occurs on the Φ scale can be achieved by examining the very extended "needle" cluster inherent structure presented in Fig. 3. This consists of a stack of 18 triangles of atoms, with a 60° twist from one to the next, and with the last particle stuck to one end. The relative minimum for this arrangement has depth:

$$\Phi_{55}(\text{needle}) = -174.129\,509\ \ldots . \tag{3.4}$$

The totality of potential energy minima is obtained by taking particle permutations into consideration. The overall number Ω of minima for Φ can be expressed formally as the sum

$$\Omega = N! \sum_{\alpha} s_{\alpha}^{-1}, \tag{3.5}$$

where α spans the *distinct* structures, and s_α denotes the symmetry number for structure α. The majority of the inherent structures for large N, and in particular for $N = 55$, will have no symmetry, i.e., $s_\alpha = 1$. However the special structures shown in Figs. 1, 2, and 3, respectively, have $s_\alpha = 60$, 24, and 3.

The process that is least costly in potential energy for separating one of the particles from the icosahedral ground state involves removal of one of the 12 vertex particles in the outer shell. After fully relaxing the resulting 54-atom cluster, the potential energy is found to be

$$\Phi_{54}(\text{vertex hole}) = -250.039\,444\ \ldots . \tag{3.6}$$

Figure 4 shows this vertex–hole arrangement.

Removal of the vertex particle appears to require no barrier crossing, so the energy shown in Eq. (3.6) is an evaporation threshold. Whenever the total cluster energy in a dynamical run exceeds this threshold it is possible in principle for the cluster of 55 particles to shed one particle. The theory of unimolecular decay rates[32] assures that the probability of occurrence of such an event per unit time is very small just above threshold but increases strongly with in-

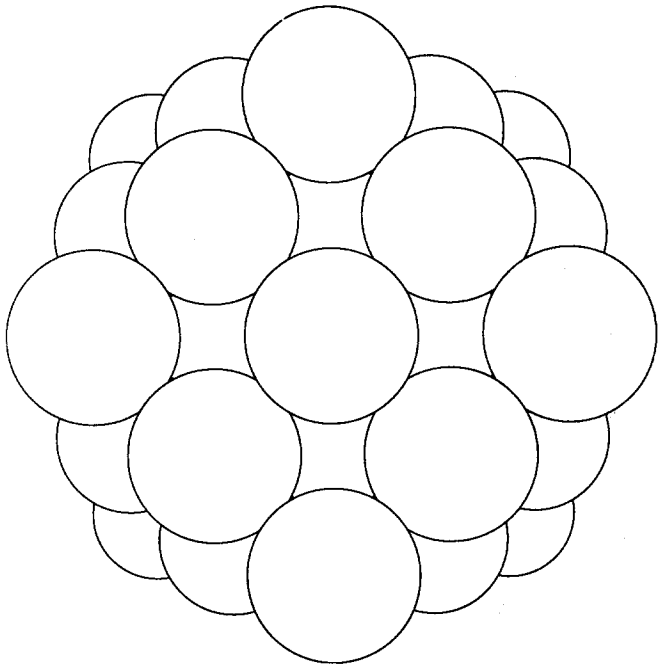

FIG. 2. Cuboctahedral inherent structure for the 55-atom cluster, substantially a fragment of the infinite fcc crystal.

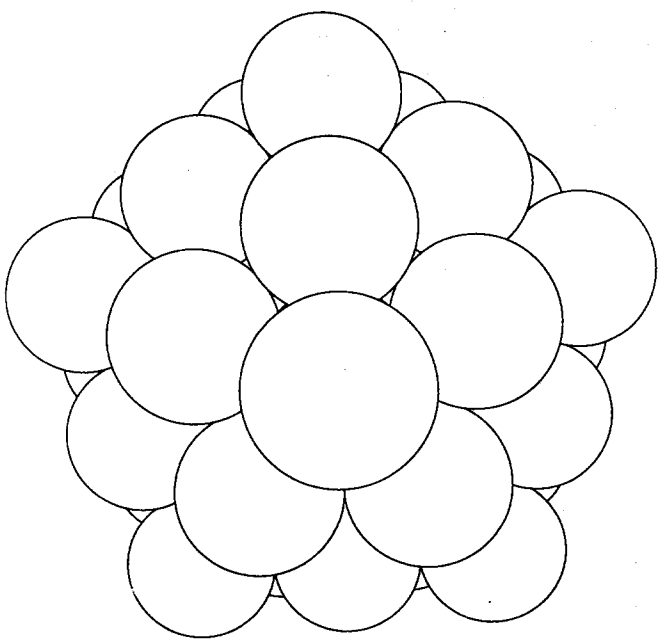

FIG. 1. Icosahedral ground state structure for the 55-atom cluster with v_5 pair interactions [Eq. (2.2)].

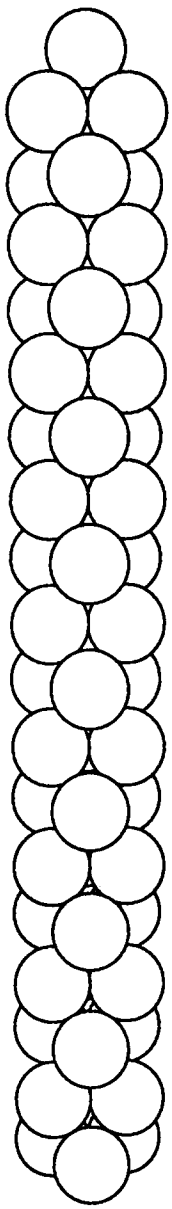

FIG. 3. High-potential energy, but mechanically stable, needle-form cluster, $N = 55$.

crease in total energy. We have taken pains to monitor the simulation dynamics so as to avoid fragmentation. Results reported in the following sections (IV, V, and VI) refer only to intact clusters.

The 30 nonvertex particles in the outer shell of the icosahedral cluster are all equivalent, and reside at the midpoints of face edges. Removing any one of these to infinity leaves a higher-potential energy structure for 54 particles with

$$\Phi_{54}(\text{edge hole}) = -247.608\,614\ \ldots . \tag{3.7}$$

Figure 5 presents the inherent structure.

Addition of a 56th particle to the $N = 55$ icosahedron (the first step in building the third shell of 92) can occur at either of two types of surface sites. The more favorable site is at the center of a triangular face, creating a 56-particle inherent structure with

$$\Phi_{56}(\text{center}) = -260.181\,464\ \ldots . \tag{3.8}$$

The alternative is occupation of any of three equivalent off-center sites on a triangular face, with

$$\Phi_{56}(\text{off-center}) = -259.889\,080\ \ldots . \tag{3.9}$$

The former particle position is legitimately part of the closed shell that completes at $N(3) = 147$, whereas the latter must be displaced to form the shell.

IV. CALORIC EQUATION OF STATE

One of the most basic statistical properties of a cluster is the way that its mean energy varies with temperature. In the present classical context this is essentially determined by the variation of mean potential energy with kinetic energy. When the total energy (with fixed center of mass) lies below the evaporation threshold shown in Eq. (3.6), the statistical average of interest requires sampling the entire bounded, classically allowed, configuration space. If the system dynamics is quasiergodic, the average should automatically emerge from the simulation provided the molecular dynamics runs are sufficiently long. However, when total energy exceeds the threshold (3.6), care must be exercised to avoid cluster fragmentation. This can become a severe problem at high temperature.

The statistical mechanical theory of physical clusters[33] suggests a definition of "intact cluster" that is useful for the

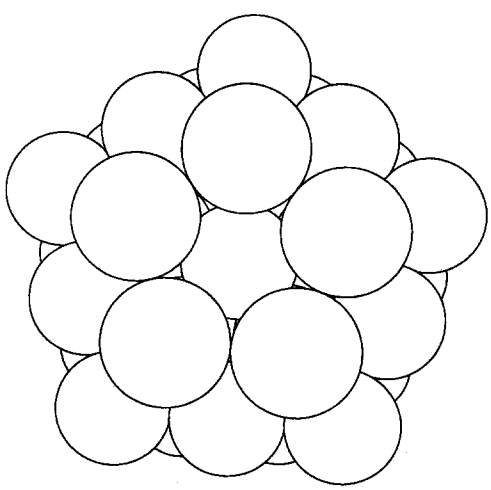

FIG. 4. Vertex–hole cluster for 54 particles.

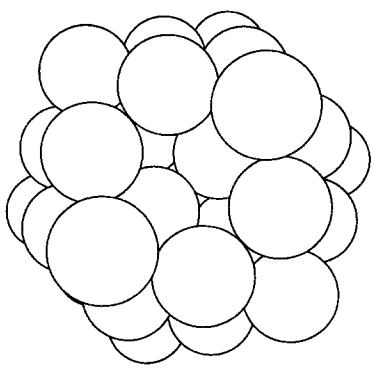

FIG. 5. Edge–hole cluster for 54 particles.

present study. One imagines that each particle is centrally surrounded by an imaginary sphere with diameter b. Overlaps of b spheres define topological connectivity, and all particle pairs within an intact cluster either must overlap directly, or be indirectly connected through a chain of overlaps. It is obvious that evaporation causes disconnection. Above threshold the desired variation of mean potential energy with kinetic energy entails sampling only the "connected" or "intact" cluster configurations.

For present purposes, the precise value of b is not crucial; it can be set equal to $2r_e$ for simplicity. It should be noted in passing that a unique b value is suggested by the general physical cluster theory, as a result of considering critical region percolation processes. During the course of our molecular dynamics runs we have tested for cluster connectivity. While particle evaporation has occurred on occasion, the results reported below refer strictly to intact cluster averages.

Figure 6 displays the caloric equation of state (mean potential vs mean kinetic energy) from a single heating sequence for the $N = 55$ cluster. In this case the system was started at the icosahedral ground state configuration with very small particle velocities, then heated in stages. The most obvious property shown by the results is that two branches are involved, a low temperature "solid" branch and a high temperature "liquid" branch.[23] The upper limit to the solid branch is its effective instability point; this occurs at about 40 K when converted to the Ar case, to be compared with 84 K for the bulk Ar triple point temperature. Subsequent molecular dynamics heating calculations have verified that the overall behavior shown in Fig. 6 is substantially reproducible.

Each of the points appearing in Fig. 6 represents a constant-energy average of length 50τ (108 ps for Ar). Between successive points the velocities were uniformly scaled upward to raise total energy, and a 5τ equilibration period was then allowed to elapse before the next averaging interval began. The average rate of temperature rise, in Ar terms, just before and just after the melting event was quite large by conventional standards:

$$dT/dt \cong 5\times 10^9 \text{ K/s}. \tag{4.1}$$

While the system inhabits the solid branch at its lower temperature end, mapping the dynamical configuration to potential energy minima virtually always produces the icosahedral ground state, Eq. (3.2). In the higher range of the solid branch, however, the system undergoes excursions outside of the icosahedral basin into neighboring basins for higher-lying relative Φ minima. Figure 7 offers a representative case, a run at mean kinetic energy 25.032 (approximately 37 K for Ar, length 108 ps). Vertical pairs of potential energy points are plotted, corresponding to before and after the mapping-to-minima operation. Although the mapping was effected at 126 equally spaced times (every 0.861 ps for Ar), the dynamical prequench potential varies too rapidly with time to convey visually the fact that it is actually a continuous function of time. The majority of the mappings yield the icosahedral ground state, but a few are seen to lie higher in potential energy.

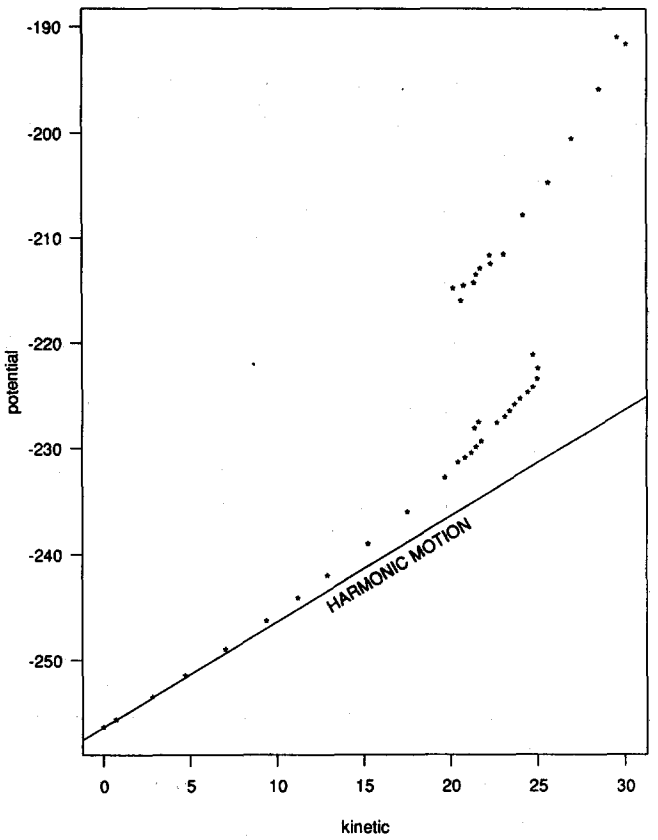

FIG. 6. Caloric equation of state for the intact 55-particle cluster. Points shown were generated during a single molecular dynamics heating sequence. The straight line, shown for reference, represents the equipartition results expected for harmonic normal modes.

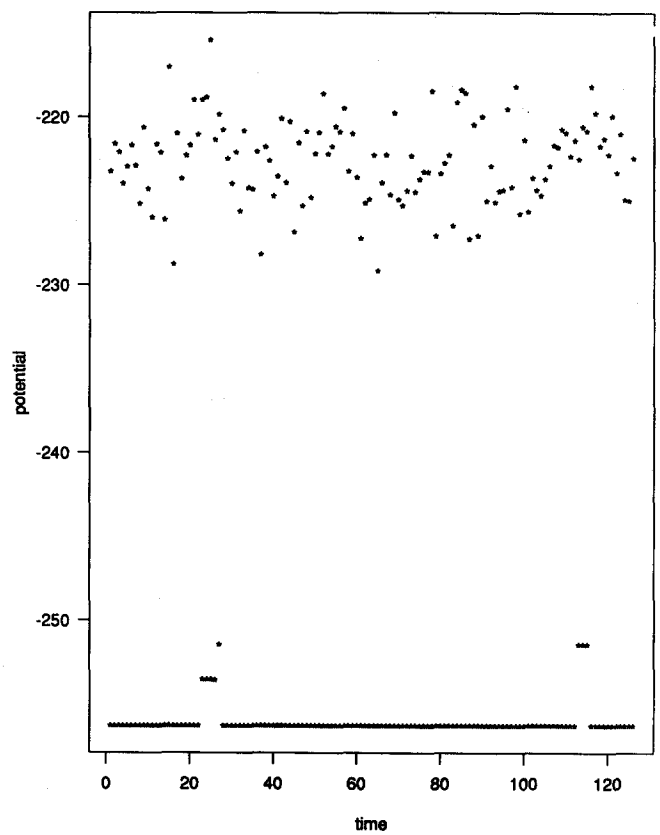

FIG. 7. Prequench and post-quench potential energies for a dynamical run along the solid branch of the caloric equation of state. The mean kinetic energy was 25.032.

The straight line included in Fig. 6 for comparison purposes would result if internal cluster motions were those of harmonic normal modes, i.e., it is the appropriate equipartition line. Results in Fig. 6 obviously deviate substantially above this harmonic normal mode base line, thus demonstrating the influence of strong anharmonicity. It must be stressed that this reflects predominately intrabasin anharmonicity for the icosahedral ground state. Only near the upper temperature end of this branch does anharmonicity due to interbasin transitions begin to contribute substantially. The two anomalous high points along the solid branch at kinetic energy about 22–23 were dominated by long interbasin excursions, while in other heating circumstances such cases do not appear as prominently.

Figures 8 and 9 present a prequench and post-quench configuration pair from the run illustrated in Fig. 7. These correspond to the last of the lower structural excitations in that diagram, with inherent structure potential energy

$$\Phi = -253.563\,714\ \ldots . \tag{4.2}$$

Substantial vibrational amplitude is present in the prequench configuration of Fig. 8, making its description and identification ambiguous at best. However, removal of vibrational distortion by the mapping amounts to a powerful image enhancement tool. The post-quench configuration displayed in Fig. 9 should be described unambiguously as a "particle, vertex–hole" structural excitation (cf. Fig. 4). The higher excitations in Fig. 6 can similarly be identified as "particle, edge–hole" structures.

Results of mapping from the liquid branch differ in two primary respects in comparison with those from the solid branch. First, the minima encountered are substantially higher. Second, the amount of time that the system spends within any basin tends to be much shorter. Figure 10 illustrates these features with prequench and post-quench potential energy pairs from a liquid-branch run with mean kinetic energy equal to 28.532 (42 K for Ar). Only a small fraction of the successive pairs of quench potential energies show no change.

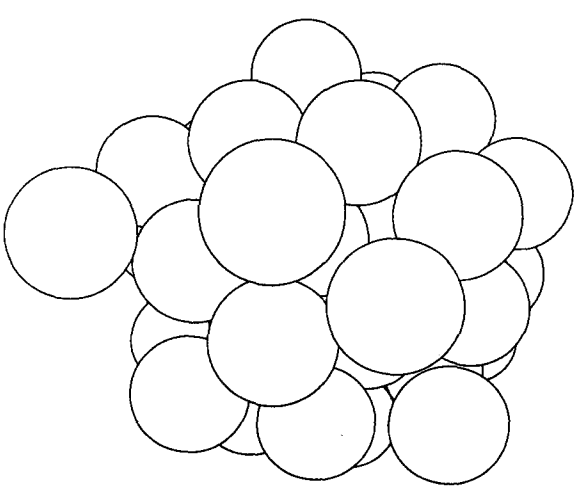

FIG. 8. Prequench cluster configuration from the molecular dynamics run of Fig. 7.

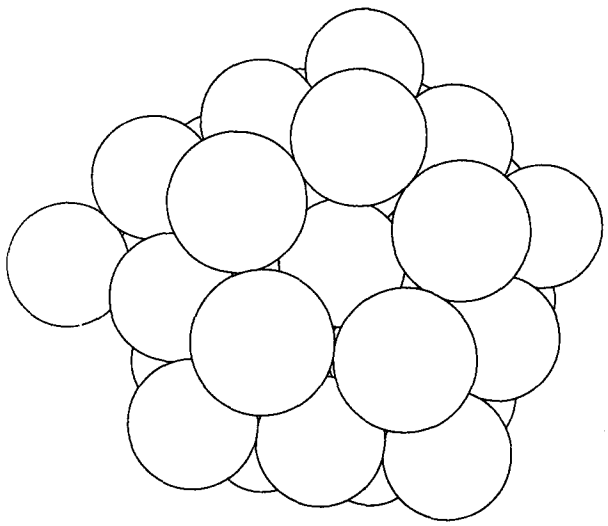

FIG. 9. Post-quench cluster configuration resulting from the mapping of the Fig. 8 configuration. The structure shown is a "particle, vertex–hole" excitation, with $\Phi = -253.563\,714\ \ldots$.

Figure 11 exhibits a typical amorphous quench structure obtained from the low temperature end of the liquid branch. This specific case was generated during a run with mean kinetic energy equal to 20.061. In spite of the image-sharpening capacity of the mapping, this inherent structure defies simple description as a slightly mutated descendant of the icosahedral Mackay polyhedron. Its potential energy is $-240.772\,516\ \ldots$.

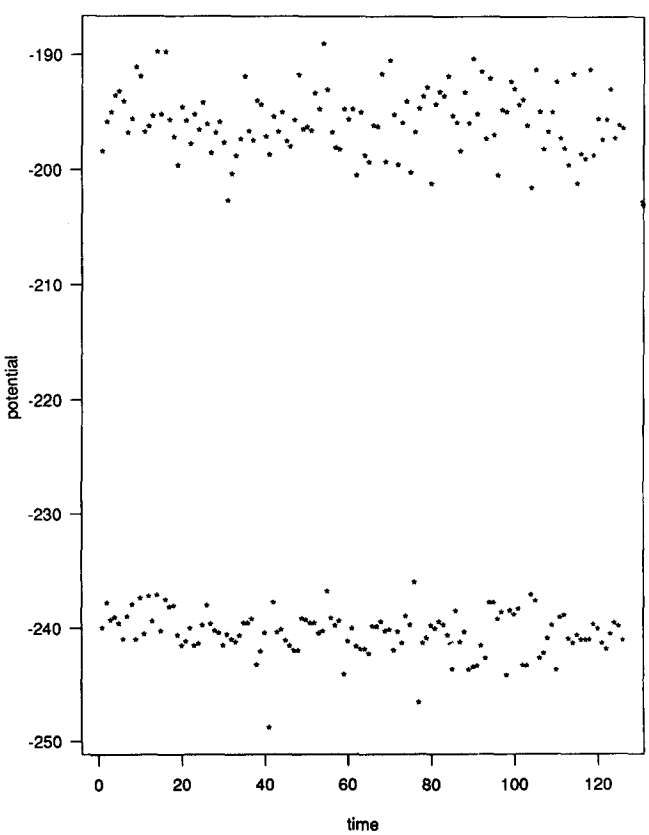

FIG. 10. Prequench and post-quench potential energies for a dynamical run along the liquid branch of the caloric equation of state. The mean kinetic energy was 28.532.

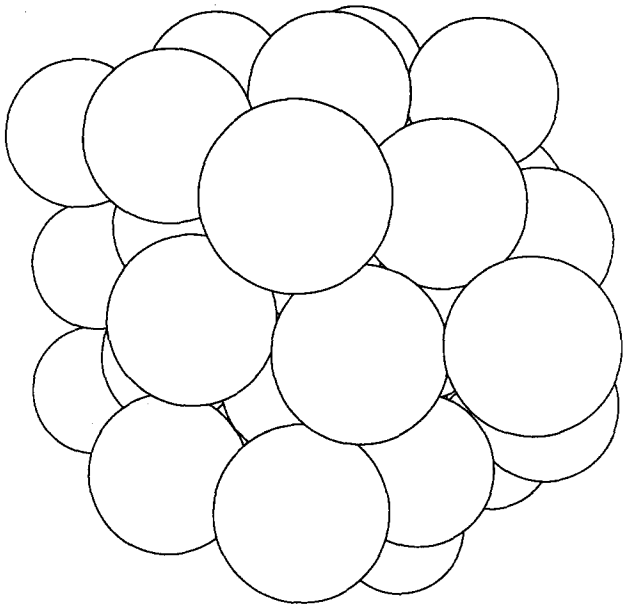

FIG. 11. Typical cluster inherent structure from the low-temperature end of the liquid branch. The potential energy at this relative minimum is $-240.772\,516\ldots$.

As temperature rises along the liquid branch, the inherent cluster structures tend to become less compact and to have higher potential energies. Figure 12 offers an example from the run with mean kinetic energy 28.532. This structure is clearly less compact than the one shown in Fig. 11. Its potential energy is $-235.876\,827\ldots$. These changes can be described as due to the excitation of surface capillary waves on the liquid droplet,[34,35] with the implication that such waves largely survive the mapping operation.

The vertical displacement between the solid and liquid branches in Fig. 6, in the neighborhood of the transition, is approximately 16.0 energy units. The average of the kinetic energies at the upper extremity of the solid branch and at the lower extremity of the liquid branch is 22.5. This corresponds to a reduced temperature [see Eq. (2.7)]:

$$T_m^* = 2(22.5)/3(54) = 0.278, \tag{4.3}$$

which we take as the effective thermodynamic melting temperature for the small cluster. This is equivalent to 33.3 K for Ar. The change in entropy that attends melting is then estimated to be

$$\Delta S/k_B \cong 16.0/0.278 = 57.6. \tag{4.4}$$

The exponential of this result represents the factor by which the inhabited configuration space expands upon melting:

$$\exp(\Delta S/k_B) \cong 9.89\times 10^{24}. \tag{4.5}$$

In part, this large number reflects the fact that only a few low-lying basins are inhabited along the solid branch, while probably a substantial fraction of the total becomes accessible after melting. It also probably reflects lower mean restoring forces for amorphous vs icosahedral basins.

By two simple measures, the extent of anharmonicity along the solid and liquid branches in Fig. 6 is comparable. First, the rising-slope trend with increasing temperature exhibited along the solid branch appears essentially to be continued (even in approximate magnitude) across the melting discontinuity onto the liquid branch. Second, the mean reduction in potential energy resulting from quenching to minima is approximately the same (26.5 energy units) at T_m^* whether the quenching occurs from the solid branch or the liquid branch.

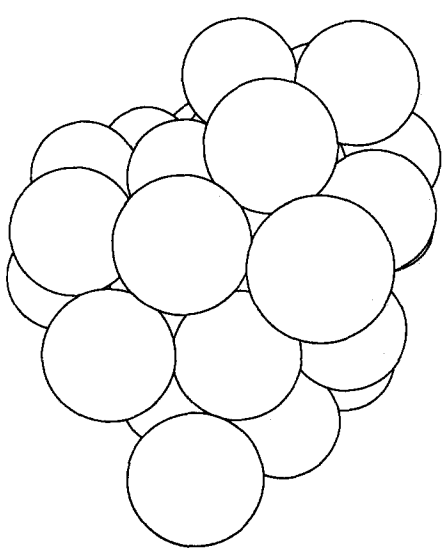

FIG. 12. Cluster inherent structure from the higher temperature region of the liquid branch. The corresponding potential energy is $-235.876\,827\ldots$.

V. PHASE TRANSITION DYNAMICS

The existence of a temperature range in Fig. 6 over which both solid and liquid branches of the caloric equation of state can be identified indicates a phase bistability phenomenon. This situation has been noted and discussed before, and is particularly noticeable for magic number clusters.[23] Within that temperature range, a constant-energy simulation of sufficient length will show occasional rapid transitions between extended periods of solid-like cluster behavior and of liquid-like cluster behavior. On account of the positive melting energy, kinetic temperature shows a higher mean value during solid-like intervals in a given molecular dynamics run than during the liquid-like intervals. The fraction of time spent in each of these phases must vary smoothly (though rapidly) across the coexistence temperature interval. Lengthy molecular dynamics simulations should represent these fractions accurately and should in principle produce a single continuous curve for the caloric equation of state. The effective cluster melting temperature T_m^* would correspond to that cluster energy which yields equal times in the two states.

The technique of mapping the dynamical cluster configuration onto potential energy minima offers a new way to examine the dynamics of transitions between solid and liquid forms. Figure 13 shows a short interval of 0.80τ (1.72 ps for Ar) during which a melting event occurred. Pairs of prequench and post-quench potential energies are presented as before, but now the mapping is so frequent that the continuous nature of the dynamical potential energy is obvious. This melting event occurred during an equilibration run in

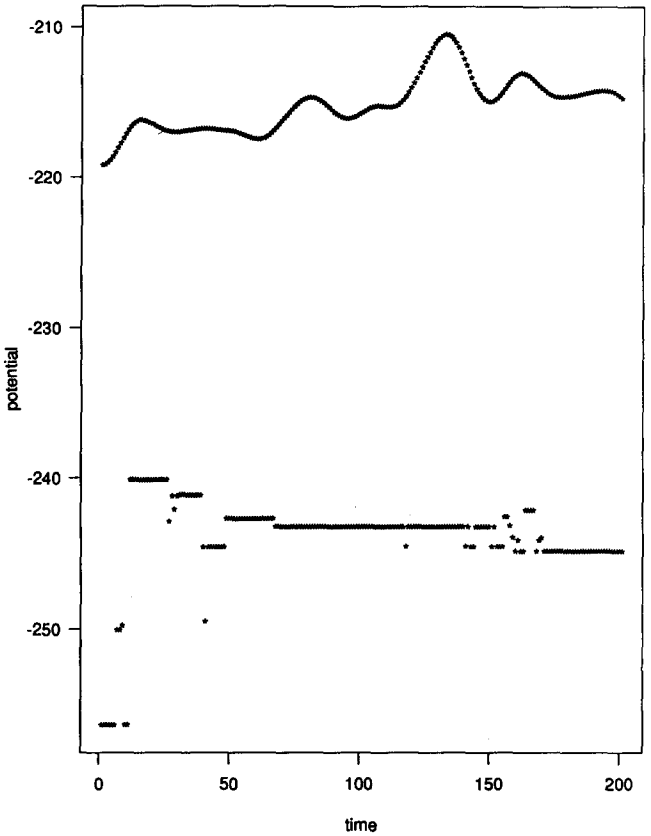

FIG. 13. Short dynamical sequence (0.80τ, 1.72 ps for Ar) during which a melting event occurred. The initial configuration during the interval shown has the system within the icosahedral ground state basin.

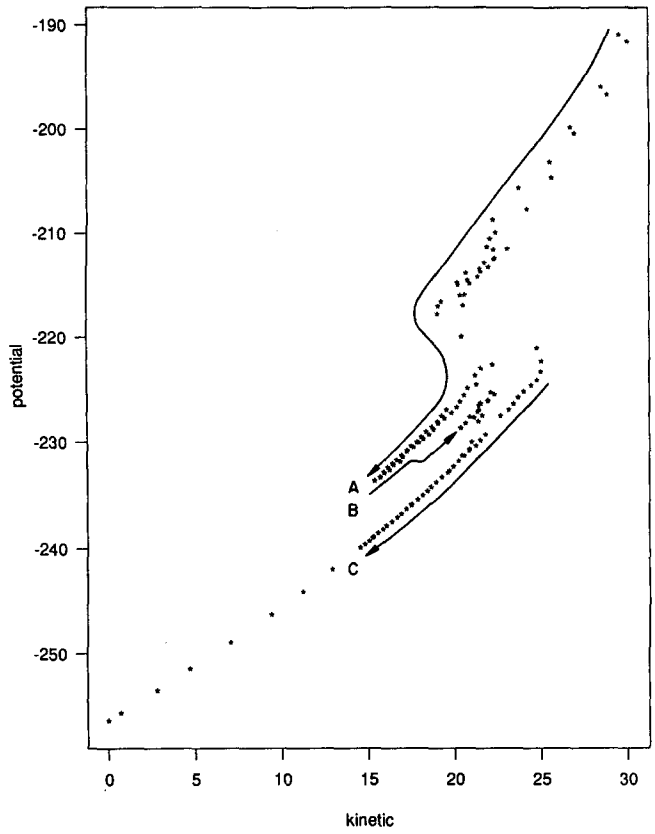

FIG. 14. Cooling and annealing sequence, starting with a warm liquid droplet, and ending on the icosahedral ground state branch.

the heating sequence represented in Fig. 6, between the last solid-branch and first liquid-branch points of that earlier graph. During the short interval of Fig. 13, the system began its dynamics within the ground-state basin, momentarily flickered across boundaries of higher-lying basins with $\Phi \cong -250.0$, returned briefly to the ground-state basin, then went *directly* into a group of higher-lying amorphous-structure basins. In particular, the system was able to bypass the low-lying particle–hole structural excitations. Evidently the icosahedral ground state basin shared bounding hypersurfaces with a wide range of other classes of basins. During other melting events, the particle–hole states do indeed make a momentary appearance.

Time reversal symmetry implies that the scenario shown in Fig. 13 could in principle run backward for a freezing event. In practice, some hysteresis is probable and a more diverse set of scenarios is available. Just as in the freezing of real melts in bulk, we have observed an initially liquid-state cluster to freeze in stages, first to an imperfect solid, and then, by rejecting defects during an annealing state, to the structurally perfect ground state. Figure 14 shows a plot of mean potential energy vs mean kinetic energy during a sequence of molecular dynamics runs that started with a warm liquid droplet, cooled it stepwise through an imperfect freezing, applied a warming subsequence to produce some annealing, then cooled slowly (with a final annealing event) to retrace finally the icosahedral ground-state branch.

By carrying out quenches to minima and examining the resulting cluster configurations, it became clear that the first solidification state in Fig. 14 placed the cluster in a set of basins corresponding to two-particle, two-vertex–hole configurations. Figure 15 illustrates one of these configurations, with $\Phi = -251.720\,646\ldots$. Notice that the vacant vertices are neighbors, with a shared particle in their respective pentagonal margins. Also notice that the two particles pro-

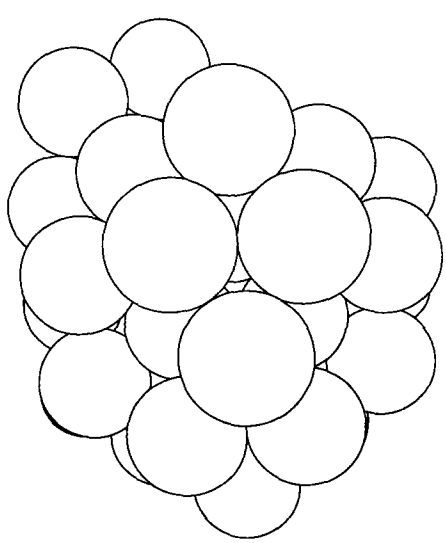

FIG. 15. Two-particle, two-vertex–hole cluster configuration. Note that the two pentagonal vertex holes share a pentagon vertex, and that the two particles promoted to the next shell are a bound pair.

moted to the next shell form a bound pair. While the system remained on this defective solid branch, several distinct two-particle, two-vertex–hole states appeared, all confined to a narrow band of local-minimum potentials.

Figures 16 and 17 display prequench and post-quench potential energies during time intervals that yielded the two annealing events. The first of these occurred during heating and shows the system dropping from the two-particle, two-vertex–hole band to the one-particle, one-vertex–hole band. The second of these occurred during subsequent cooling, and records the system exiting the one-particle, one-vertex–hole band to take up residence in the icosahedral ground state basin.

We believe that our quenching studies have been sufficiently complete to detect and classify all inherent cluster structures in the one-particle, one-vertex–hole band. Eleven such structures have been found. Their energies are known to high accuracy, and are listed in Table II, as well as illustrated in "line spectrum" form in Fig. 18. The 11 structures divide into two groups depending on whether the promoted particle sits over the center of an icosahedron face (four structures), or sits in an off-center site (seven structures). "Unperturbed" energies for each of these groups can be achieved by combining 54, 55, and 56 particle potential energies from Sec. III under the assumption that the hole and the particle are noninteracting. For the centered-particle group we have the estimate

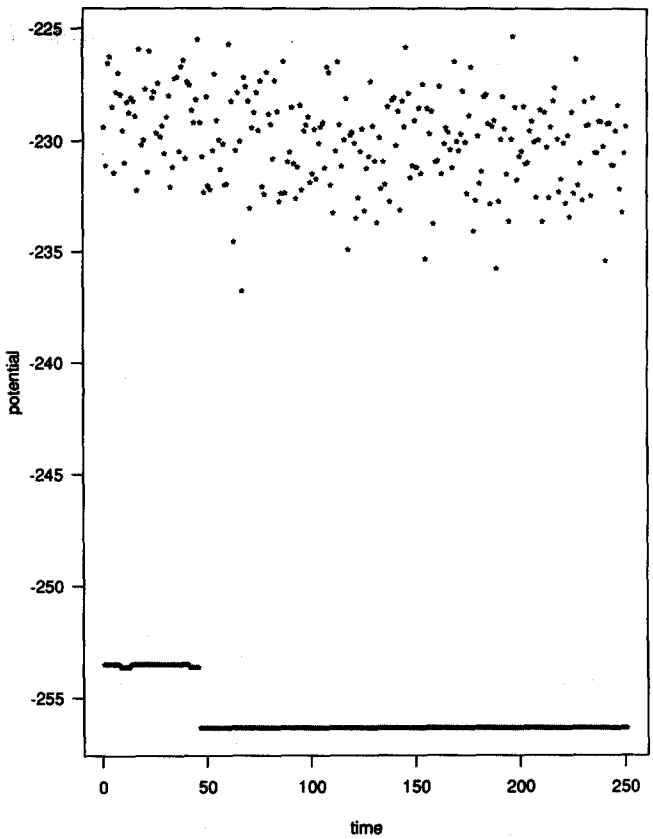

FIG. 17. 50τ time interval during which the imperfect cluster in the one-particle, one-vertex–hole band annealed into the icosahedral ground state basin.

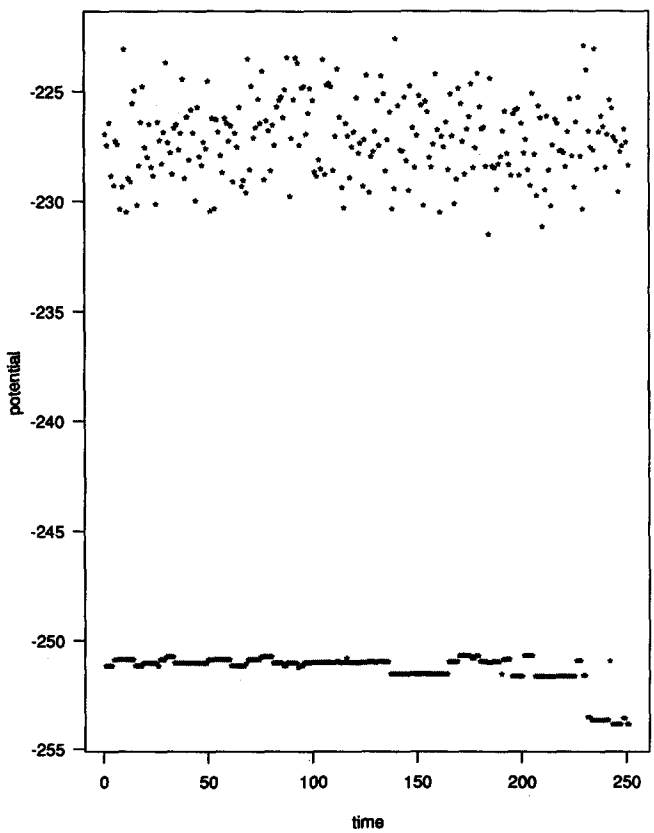

FIG. 16. 50τ time interval during which the imperfectly frozen cluster annealed from the two-particle, two-vertex–hole band to the one-particle, one-vertex–hole band.

$$\Phi_{54}(\text{vertex hole}) + \Phi_{56}(\text{center}) - \Phi_{55}(\text{icos}) = -253.858\,637\ \ldots . \quad (5.1)$$

Similarly, for the off-center group we have

$$\Phi_{54}(\text{vertex hole}) + \Phi_{56}(\text{off-center}) - \Phi_{55}(\text{icos}) = -253.566\,253\ \ldots . \quad (5.2)$$

These unperturbed values lie within the limits for the respective groups and are indicated by dotted lines in Fig. 18.

In fact, two types of perturbations are present to split the unperturbed energies (5.1) and (5.2) into the observed levels. The larger perturbation is the missing pair interaction, if particle and hole are within the interaction range a, that

TABLE II. Potential energies of inherent cluster structures in the one-particle, one-vertex–hole band.

Off-center-particle states:	
	−253.519 377 96
	−253.563 714 94
	−253.566 642 17
	−253.567 105 26
	−253.567 548 79
	−253.568 563 51
	−253.570 840 31
Centered-particle states:	
	−253.655 465 66
	−253.857 335 48
	−253.860 067 27
	−253.860 307 38

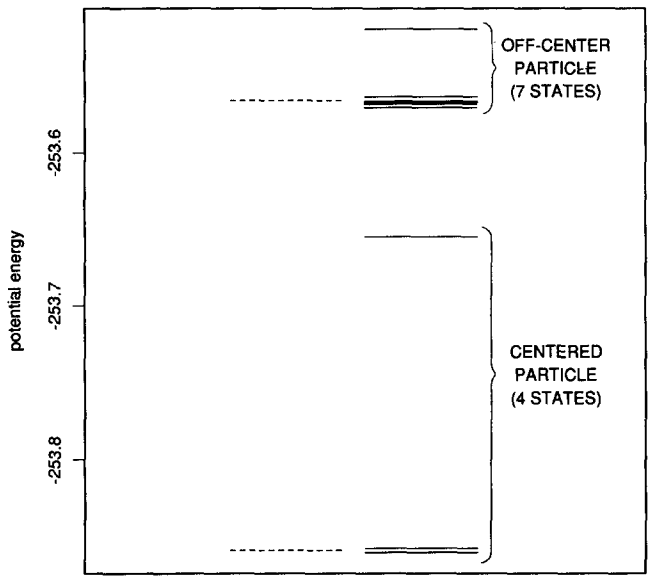

FIG. 18. Line spectrum for inherent cluster structure energies in the one-particle, one-vertex–hole band. Precise energies for the 11 states appear in Table II. Dotted lines are "unperturbed" energies for the two groups of states.

would be present if the vertex hole were filled. Indeed, cluster pictures have demonstrated that the highest level in each group exhibits the closest approach between particle and vertex hole. The other, and much weaker, perturbation involves elastic deformation of the cluster. If either a vertex hole alone ($N=54$) or an extra particle alone ($N=56$) is present the icosahedral symmetry initially exhibited by the other particles is broken. This has the effect of making inequivalent the vertex–hole or excess particle sites that were identical in the icosahedron ($N=55$).

VI. GENERALIZED LINDEMANN CRITERIA

The Lindemann melting criterion for crystalline solids, originally proposed in 1910, has become a particularly useful and quantitatively reliable rule for locating the melting points of atomic substances.[36,37] Its conventional exposition involves the ratio of rms particle displacements from lattice sites to the nearest-neighbor spacing l:

$$\lambda(T) = \langle(\delta\mathbf{r}_i)^2\rangle^{1/2}/l. \tag{6.1}$$

Melting usually occurs when $\lambda(T)$ rises with increasing temperature to approximately the following magnitude:

$$\lambda(T_m) \cong 0.15. \tag{6.2}$$

Solid He^4 and the electron-gas Wigner lattice are probably exceptional, with substantially larger $\lambda(T_m)$ due to extreme quantum effects.[38]

The inherent structure formalism trivially re-interprets $\delta\mathbf{r}_i$ as the displacement of particle i during mapping of the system configuration to the relevant local minimum of Φ. As a result, $\lambda(T)$ in Eq. (6.1) is automatically defined for *both* crystal and liquid phases since the mapping procedure is available regardless of what phase of matter is involved. This extension automatically leads to a freezing criterion for liquids that complements the Lindemann melting criterion.[25] Molecular dynamics simulation reveals that $\lambda(T)$ is substantially larger in the liquid than in the crystal and rises with increasing temperature. Upon cooling, the liquid becomes unstable with respect to nucleation and crystallization when $\lambda(T)$ declines to about 0.4.

It is natural to examine $\lambda(T)$ for the 55-atom cluster and to relate the solid and liquid branch values at the melting point to those found in extended condensed phases. Figure 19 presents results for $\langle(\delta\mathbf{r}_i)^2\rangle^{1/2}$, the rms quenching displacements for selected thermodynamic states of the cluster. As expected, the behavior of the solid branch in the low temperature limit reflects a square-root singularity in kinetic energy, i.e., in temperature. The rms displacement rises to a limit of about 0.14 at T_m^* (where the mean kinetic energy is 22.5). The limiting value of the liquid-branch rms displacement at T_m^* is approximately 0.29.

For this cluster application l should be taken to be the mean nearest-neighbor separation in the icosahedral ground state:

$$l = 1.10. \tag{6.3}$$

This choice leads to the following Lindemann-type melting and freezing criteria for the 55-atom cluster:

$$\lambda_s(T_m^*) = 0.13, \quad \lambda_l(T_m^*) = 0.26. \tag{6.4}$$

Here "s" and "l" refer to "solid" and "liquid," respectively. These values are both smaller than the corresponding bulk

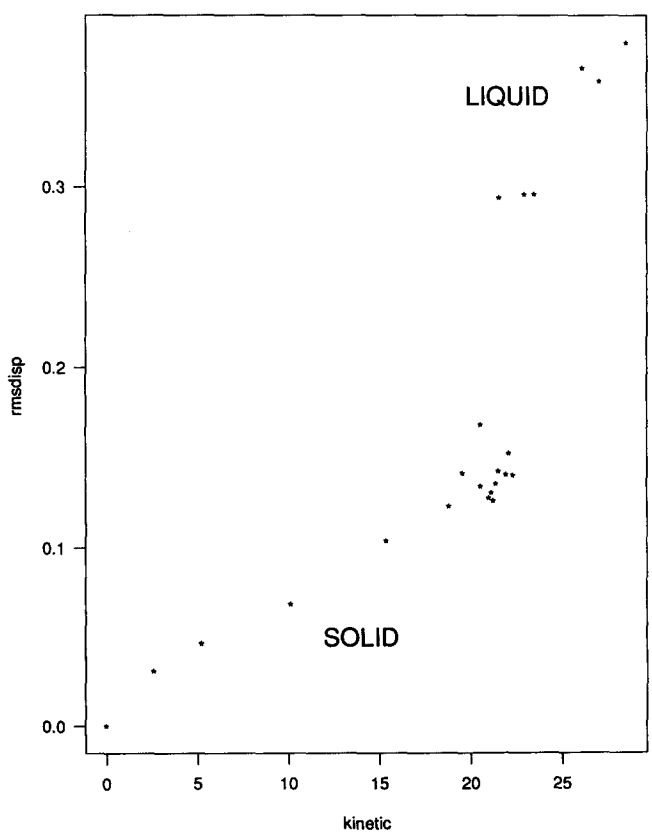

FIG. 19. Root-mean-square displacements of particles resulting from mapping to minima vs cluster kinetic energy.

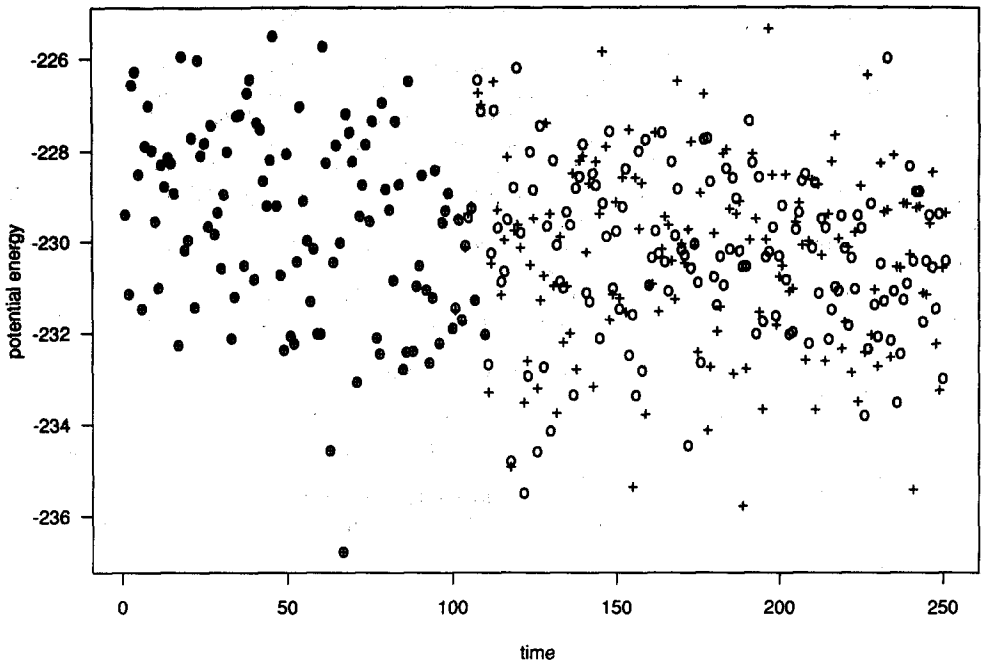

FIG. 20. Potential energies sampled along a pair of chaotic liquid-droplet trajectories (denoted by O and +, respectively) of length 50τ. The initial conditions for the trajectories were identical except for a displacement of one coordinate of one particle by approximately 1 part in 10^{16}. Exponential divergence of the trajectories becomes visibly obvious in this potential plot after about 20τ have elapsed. Mean kinetic energy was approximately 21.

phase quantities (0.16 and 0.44, respectively[25]), showing the effect of the small system size for the cluster.

It would be instructive to see eventually if analogous calculations for larger and larger Mackay polyhedral clusters smoothly converge onto the bulk phase values of $\lambda_s(T_m^*)$ and $\lambda_l(T_m^*)$.

VII. DISCUSSION

Coupling conventional molecular dynamics simulation with the mapping to potential-energy local minima, the inherent structures, creates a powerful tool for analyzing many-body phenomena. The preceding text illustrates that point for the case of the 55-atom cluster, particularly regarding its phase transition behavior. In this connection one can ask about the role of the cuboctahedral cluster fragment of the fcc lattice, Fig. 2, which Sec. III points out is a locally stable 55-atom entity. One might have expected it to be encountered as a quench result during study of cluster dynamics. Considering its energy, Eq. (3.3), its basin could in principle be an occasional contributor to the liquid droplet form of the cluster. In fact, we have searched in vain through thousands of quench potentials generated in the course of our simulations and have never seen the cuboctahedral structure spontaneously appear. In view of the order of magnitude estimated in Sec. III for the total number of distinct inherent structures for $N = 55$, this negative result may not be very surprising.

Considering the fact that substantial anharmonicity exists in the liquid droplet branches for both the caloric equation of state and the rms displacements, it should come as no surprise that the dynamics is clearly chaotic there. The presence of at least one positive Liapunov exponent[39] can be, and has been, demonstrated by a simple numerical expedient. By changing the initial position of one particle by approximately one part in 10^{16} for a 50τ run at mean kinetic energy of about 21, the final configuration becomes drastically altered. Figure 20 provides an example. This occurs with virtually no change in the conserved energy. By comparing, side by side, the configurations of particles during a pair of such runs in this temperature range differing only by that initial tiny perturbation, it is clear that the configurational discrepancy between the two grows exponentially with time. By contrast, no such trajectory divergence occurs when a similar initial-state perturbation is applied to the cold icosahedral cluster (with mean kinetic energy approximately 3).

Some variant of unimolecular decomposition rate theory[32] doubtless could be devised to calculate evaporation rates of particles from the icosahedral ground state structure. However, this would only be relevant to the 55-atom cluster at low temperature, where the evaporation process is too slow to observe during molecular dynamics simulation. By contrast, molecular dynamics is well suited to determine evaporation rates from the higher temperature liquid droplet state and it would be valuable to carry out a systematic study of this phenomenon in the future. The results would benefit understanding of accommodation (sticking) coefficients and thus understanding of cluster growth and decay processes in the vapor phase.

[1]R. P. Andres *et al.*, J. Mater Res. **4**, 704 (1989).
[2]M. L. Steigerwald and L. E. Brus, Ann. Rev. Mater. Sci. **19**, 471 (1989).
[3]K. Liu, E. K. Parks, S. C. Richtsmeier, L. G. Probo, and S. J. Riley, J. Chem. Phys. **83**, 2882, 5353(E) (1985).
[4]A. Faibis, E. P. Kanter, L. M. Tack, E. Bakke, and B. Zabranski, J. Phys. Chem. **91**, 6445 (1987).
[5]D. Turnbull, in *Solid State Physics*, edited by F. Seitz and D. Turnbull (Academic, New York, 1956), Vol. 3, pp. 225–306.
[6]F. F. Abraham, *Homogeneous Nucleation Theory* (Academic, New York, 1974).
[7]A. Kaldor, D. M. Cox, and M. R. Zakin, Adv. Chem. Phys. **70** (part 2), 211 (1988).
[8]K. Raghavachari and C. M. Rohlfing, J. Chem. Phys. **89**, 2219 (1989).
[9]C. M. Rohlfing and K. Raghavachari, Chem. Phys. Lett. (in press).
[10]W. L. Brown, R. R. Freeman, K. Raghavachari, and M. Schluter, Science **235**, 860 (1987).

[11]H. W. Kroto, J. R. Heath, S. O'Brian, R. F. Curl, and R. E. Smalley, Nature **318**, 162 (1985).
[12]F. H. Stillinger and R. A. La Violette, J. Chem. Phys. **83**, 6413 (1985).
[13]F. H. Stillinger and R. A. La Violette, Phys. Rev. B **34**, 5136 (1986).
[14]R. A. La Violette and F. H. Stillinger, J. Chem. Phys. **85**, 6027 (1986).
[15]R. A. La Violette, Phys. Rev. B (in press).
[16]A. L. Mackay, Acta Crystallogr. **15**, 916 (1962).
[17]F. H. Stillinger and T. A. Weber, Kinam A **3**, 159 (1981).
[18]F. H. Stillinger and T. A. Weber, Phys. Rev. A **25**, 978 (1982).
[19]F. H. Stillinger and T. A. Weber, Phys. Rev. A **28**, 2408 (1983).
[20]T. A. Weber and F. H. Stillinger, J. Chem. Phys. **80**, 438 (1984).
[21]F. G. Amar and R. S. Berry, J. Chem. Phys. **85**, 5943 (1986).
[22]T. L. Beck and R. S. Berry, in *The Physics and Chemistry of Small Clusters*, edited by P. Jena, B. K. Rao and S. N. Khanna (Plenum, New York, 1987).
[23]J. D. Honeycutt and H. C. Andersen, J. Phys. Chem. **91**, 4950 (1987).
[24]J. L. Garzón, M. Avalos Borja, and E. Blaisten-Barojas, Phys. Rev. B **40**, 4749 (1989).
[25]R. A. La Violette and F. H. Stillinger, J. Chem. Phys. **83**, 4079 (1985).
[26]J. O. Hirschfelder, C. F. Curtiss, and R. B. Bird, *Molecular Theory of Gases and Liquids* (Wiley, New York, 1954), p. 1041.
[27]C. W. Gear, *Numerical Initial-Value Problems in Ordinary Differential Equations* (Prentice-Hall, Englewood Cliffs, 1971).
[28]H. J. C. Berendsen and W. F. van Gunsteren, in *Molecular-Dynamics Simulation of Statistical-Mechanical Systems*, edited by G. Ciccotti and W. G. Hoover (North Holland, New York, 1986), pp. 43–65.
[29]L. C. Kaufmann (private communication).
[30]M. R. Hoare, Adv. Chem. Phys. **40**, 49 (1979); see Table I, p. 91.
[31]J. Xie, J. A. Northby, D. L. Freeman, and J. D. Doll, J. Chem. Phys. **91**, 612 (1989).
[32]K. J. Laidler, *Theories of Chemical Reaction Rates* (McGraw–Hill, New York, 1969), Chap. 6.
[33]F. H. Stillinger, J. Chem. Phys. **38**, 1486 (1963).
[34]F. P. Buff, R. A. Lovett, and F. H. Stillinger, Phys. Rev. Lett. **15**, 621 (1965).
[35]J. D. Weeks, W. van Saarloos, D. Bedeaux, and E. Blokhuis, J. Chem. Phys. **91**, 6494 (1989).
[36]F. A. Lindemann, Z. Phys. **11**, 609 (1910).
[37]J. P. Hansen and J. R. McDonald, *Theory of Simple Liquids* (Academic, New York, 1976), Sec. 10.6.
[38]S. T. Chui, Phys. Rev. B **41**, 796 (1990).
[39]J. P. Eckmann and D. Ruelle, Rev. Mod. Phys. **57**, 617 (1985).